Hydrodynamics of flow through living shoreline structure

Kanyarat Tanhaseng[1], Duangrudee Kositgittiwong[2], Chaiwat Ekkawatpanit[2], Wongnarin Kompor[2], and Chanchai Petpongpan[2]*
[1,2] Department of Civil Engineering, Faculty of Engineering, King Mongkut's University of Technology Thonburi, Bangkok, THAILAND

Abstract. Globally, the deployment of artificial seadomes has garnered increasing attention for enhancing recreational activities and providing coastal protection. The strategic placement of seadomes on the seafloor alters local hydrodynamic patterns, which play a crucial role in mitigating coastal erosion. A comprehensive understanding of these flow dynamics is essential for optimizing the design and configuration of artificial seadomes. This study presents a numerical investigation into the hydrodynamics of artificial seadomes, focusing on performance optimization by varying key parameters such as water depth (h), incident wave height (Hi), and wavelength (L). A series of 40 controlled numerical tests was conducted with seadomes arranged in five shore-parallel rows near the shoreline. The analysis reveals that a relative structure height (D/h) exceeding 1.0, coupled with a relative wavelength (L/Be) between 0.5 and 1.0, leads to wave amplitude reductions of over 90%. Larger seadomes, with widths ranging from 45 to 60 cm, achieved wave reduction rates of up to 98%. The study also explored a zig-zag formation using 3D computational fluid dynamics (CFD) with the RNG k-ε turbulence model, offering detailed insights into the flow behavior around the structures. Furthermore, a nomogram was developed as a practical tool to optimize seadome placement for enhanced wave attenuation and coastal defense. These results provide valuable guidance for future applications of artificial seadomes in real-world coastal protection efforts.

1 Introduction

A hemispherical reef is a semi-submerged or underwater structure that is widely used as a means of beach protection and beach stabilization[1-2]. There are multiple functions and opportunities for environmental enchantment, aesthetic, and wave protection in coastal areas as well as improvements of the local surfing climate biological amenities[3]. Among these characteristics are the ability to promote water circulation and provide a fish habitat enhancement capability[4]. Most of the hemispherical reefs were constructed using rocks or specially designed prefabricated concrete blocks to dissipate wave energy[5-6]. Introducing hemispherical reefs, a newly designed marine structure, which has been evaluated for its capability to attenuate surface waves in the nearshore zone for coastal protection purposes.

Over 2600 laboratory tests demonstrated that using a standard array of 5 shore-parallel rows of hemispherical reefs can achieve a wave height reduction ranging from 20% to 80% [7]. Purposed for use as a submerged composite breakwater, an array of perforated hollow hemispherical-shaped artificial reefs was chosen. Hollow hemispherical shapes were selected for their hydraulic stability, ability to reduce the tearing of fishing nets, creation of coherent eddies with upward flow, and provision of hiding places for fish[8]. An attractive

* Corresponding author: duangrudee.kos@kmutt.ac.th

characteristic of habitat structures is the ability of the hemispherical reefs to generate beneficial vortices and turbulence, as fish abundance is influenced by current vortices[9].

Proper water circulation and velocity promote the increased renewal of nutrients beneficial for larval settlement while decreasing sedimentation[10]. Sedimentation is detrimental to life because it hinders, among other factors, the renewal of nutrients and dissolved gases. Two mechanisms contribute to the stabilization of shorelines through submerged breakwaters wave attenuation and wave refraction[11]. These mechanisms will be elaborated on in the subsequent paragraphs. Even if waves do not dissipate upon the submerged breakwaters, they continue to contribute to shoreline stabilization through the effects of wave refraction. When waves break at an oblique angle to the shoreline, they induce the formation of an alongshore current capable of sediment transport along the coastal area.

In this study, the model simulation has been simulated to generate a wave interacting with the hemispherical reef structures and develop a semi-empirical formula to predict the performance of the hemispherical reef structure in attenuating surface waves. The use of a semi-empirical formula can help in the practical design of hemispherical reefs by determining the minimum structure height to water depth ratio and relative wavelength to structure width required to achieve a certain level of wave amplitude reduction, since their efficiencies in reducing wave height and wave attenuation after breaking, on the other hand, related to the shape, dimension, and arrangement of geometric.

2 Literature Review

2.1 Hydrodynamic of submerged breakwaters

Submerged breakwaters effectively reduce wave energy through wave refraction, reflection, and attenuation mechanisms[4]. Their hydrodynamic performance is governed by key parameters such as the relative crest submergence (ds/d), crest width-to-wavelength ratio (B/L), and wave steepness (Hi/L)[12]. Higher submergence depths (ds) are associated with reduced wave transmission, as wave energy dissipates primarily above the structure[5].

The shape and slope of breakwaters further influence their efficiency. Seaward-sloping designs reduce wave reflection and enhance sediment mobility, while vertical structures often lead to stronger wave rebounds and increased scouring at the base[13]. Porosity also plays a vital role permeable material, such as crushed stone, show similar energy dissipation to impermeable designs while facilitating better structural adaptability. Practical guidelines and performance charts leveraging parameters like B/L and ds/d have proven effective in evaluating submerged breakwater designs under varying environmental conditions. These insights aid in optimizing designs to maximize wave energy reduction while ensuring structural stability in high-energy coastal environments. Applied numerical modeling validated against laboratory experiments to analyze wave attenuation. Their results demonstrate that submerged breakwaters can achieve wave height reductions between 20-80%, depending on the structural configuration and wave conditions[7]. This performance highlights their viability as a coastal defense solution.

2.2 Hemispherical artificial reefs as submerged breakwaters and their application

Building upon the principles of submerged breakwaters, hemispherical artificial reefs, such as seadomes, offer unique advantages in coastal protection[5], [14]. Their geometric design enhances wave attenuation by efficiently disrupting wave energy through refraction and dissipation[15]. Compared to traditional submerged breakwaters, the semi-spherical shape promotes balanced flow dynamics, reduces scouring risks[16], and fosters ecological benefits by creating habitats for marine life. Studies have shown that hemispherical reef configurations optimize wave energy reduction by promoting uniform flow patterns and minimizing turbulence[4]. These artificial reefs have also been proven to enhance sediment deposition and stabilize the seabed, further contributing to coastal protection.

[5] Experimental study on hemispherical artificial reefs highlights the effectiveness of these structures in wave transmission reduction and sediment control, particularly under varying wave conditions. Their findings emphasize the importance of reef height, submergence level, and spacing in achieving optimal performance. By integrating hydrodynamic efficiency with ecological sustainability, semi-spherical artificial reefs address key challenges in modern coastal management and reinforce their multifunctional role in shoreline defense systems. Building upon the principles of submerged breakwaters, semi-spherical artificial reefs, such as seadomes, offer unique advantages in coastal protection. Their geometric design enhances wave attenuation by efficiently disrupting wave energy through refraction and dissipation. Compared to traditional submerged breakwaters, the semi-spherical shape promotes balanced flow dynamics, reduces scouring risks, and fosters ecological benefits by creating habitats for marine life. This innovative approach combines hydrodynamic efficiency with ecological sustainability, addressing key challenges in modern coastal management.

3 Methodology

3.1 Governing equation

In this investigation, CFD (computational fluid dynamics) is implemented. The equations solved in this context are the momentum equation, also referred to as the Navier-Stokes equation, and the continuity equation. This method is effective for resolving laminar flows. However, when it comes to turbulent flows, directly solving all the vortices in a turbulent flow is costly.

Hence, it is necessary to include a turbulence model. Multiple turbulence models are accessible. The two most prevalent models are the RANS models and big eddy simulation models. The current work employed two-equation RANS models to accurately depict the ensemble-averaged flow and simulate the impact of turbulent eddies[17]. The RANS equations involve substituting the time-averaged value for different instantaneous physical parameters. Incompressible flow is assumed accordingly, the equations are arranged as follows[18-19]:

Momentum equation

$$\rho \frac{\partial}{\partial x_j}(u_i u_j) = - \frac{\partial P}{\partial x_i} + \frac{\partial}{\partial x_j}\left(\mu \frac{\partial u_i}{\partial x_j} - \rho \overline{u'_i u'_y}\right) + S_i \quad (1)$$

Continuity equation

$$\frac{\partial u}{\partial x} + \frac{\partial v}{\partial y} + \frac{\partial w}{\partial z} = 0 \quad (2)$$

Equation (1) defines the variables used in the context: ρ represents the mass density, μ_i denotes the average velocity components for x, y, and z directions, P denotes the fluid pressure on the micro-volume, μ denotes the viscosity, μ' denotes the fluctuation velocity, and i and j=1, 2, 3 (x, y, z). Si represents the source item. In eddy viscosity turbulence models, the reynolds stresses are connected to the velocity gradients through the turbulent viscosity. This connection is referred to as the boussinesq assumption, which replaces the reynolds stress tensor in the time-averaged navier-stokes equation with the product of the turbulent viscosity and the velocity gradients. The two-equation models assume a relationship for the reynolds stresses in Eq. (1) based on eddy viscosity.

$$-\rho\overline{u_i' u_j'} = \mu_t\left(\frac{\partial u_i}{\partial x_j} + \frac{\partial u_j}{\partial x_i}\right) - \frac{2}{3}\rho k \delta_{ij} \qquad (3)$$

The renormalization group (RNG) k-εturbulence model is used in this paper. This is an enhancement to the k-ε turbulence model. The following are the new turbulence equations for k and ε[20], [21].

k equation

$$\frac{\partial}{\partial t}(\rho k) + \frac{\partial}{\partial x_i}(\rho k \overline{u_i}) = \frac{\partial}{\partial x_j}\left(\alpha_k \mu_{sff} \frac{\partial k}{\partial x_j}\right) + G_k - \rho\varepsilon \qquad (4)$$

ε equation

$$\frac{\partial}{\partial t}(\rho\varepsilon) + \frac{\partial}{\partial x_i}(\rho\varepsilon \overline{u_i}) = \frac{\partial}{\partial x_j}\left(\alpha_s \mu_{eff} \frac{\partial \varepsilon}{\partial x_j}\right) + C_{1s}\frac{\varepsilon}{k}G_k - C_{2s}\rho\frac{\varepsilon^2}{k} - R_s \qquad (5)$$

Where G_k is defined by the average flow gradient based on the turbulent kinetic energy, μ_{eff} is the validity turbulent viscosity coefficient, α_k and α_ε are the inverse turbulent Prandtl numbers for the kand ε equations, and $C_{1\varepsilon}$ and $C_{2\varepsilon}$ are known constants.

3.2 3D Model configurations

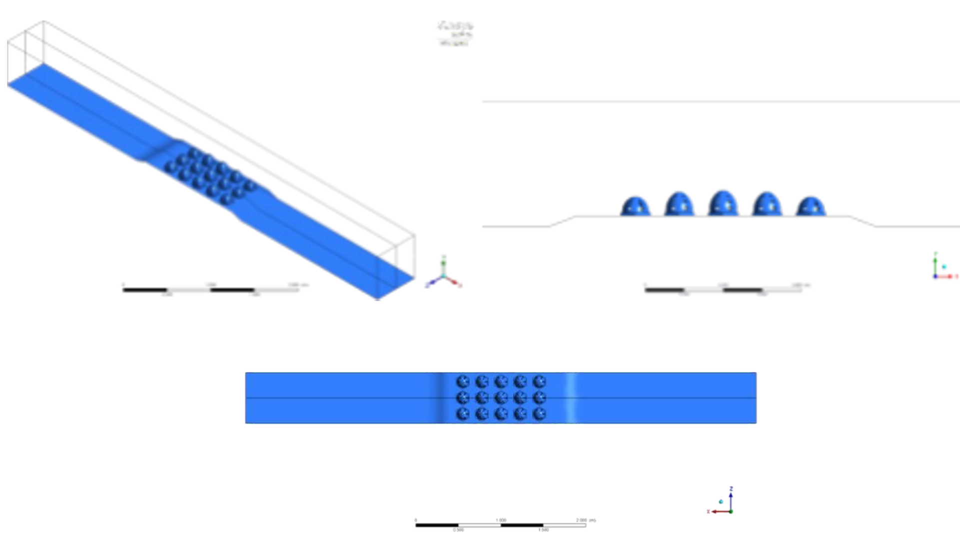

Fig.1. Schematic representation of the computation domain, which contains five rows of artificial seadome with straight alignment.

The flow field experiment for hemispherical reefs involved five distinct configurations, each comprising four different sizes and one perforated reef design. The configurations are categorized as group reef and crosswise longitudinal combination reef arrangements. Figure 1 illustrates the reef structures utilized in the study. Twelve specific flow velocities were selected, based on open channel flow theory, to simulate realistic conditions. The specifications of the simulated reef configurations were consistent with those of the physical model. The computational domain dimensions were 6 meters in length, 1.2 meters in height, and 0.6 meters in width. The setup included perforations on both sides of the reef structures, with diameters varying according to the size parameters of the artificial reefs, as depicted in figure 1.

Table 1. Governing variables and overall simulation runs

Governing variables					
Configuration	A	B	C	D	E
Size of artificial reefs	15 cm	30 cm	45 cm	60 cm	15 cm
Diameters of perforation (cm)	2.25, 1.5, 0.75 and 3	4.5, 3, 1.5 and 6	6.75, 4.5, 2.25 and 9	9, 6, 3 and 12	2.25, 1.5, and 3
Numbers of perforation	19	19	19	19	13
Width of artificial reefs (cm)	69.38	138.75	208.13	277.5	69.38
Water depth (cm)	Run1= 12.5 Run2 = 15 Run3 = 18	Run1= 25, Run2= 30.5 Run3= 36	Run1= 38 Run2= 46 Run3= 54	Run1= 50 Run2= 61 Run3= 72	Run1=12.5 Run2= 15 Run3= 18
Incident wave height (cm)	Run1= 6.87 Run2= 8.39 Run3= 9.92	Run1 = 13.74 Run2 = 16.79 Run3 = 19.84	Run1 = 20.60 Run2 = 25.18 Run3 = 29.76	Run1 = 27.47 Run2 = 33.58 Run3 = 39.68	Run1 = 6.87 Run2 = 8.39 Run3 = 9.92

Table 2. The designed parameters of seadome characteristics

Parameter	Expression	Test value	Total number applied
Selected size of Seadome	W (base width)	15, 30, ,45 and 60 cm	4
Total height of Seadome	$d_s = 0.8W$		
Thickness of basement	$t_w = 0.1W$	In accordance with the value of W	
Total height of structure array	$D = 0.925W$		
Diameters of perforations	$s_i = c_iW$	c_1=0.15;c_2=0.1; c_3=0.05;c_4=0.2	
Thickness of bedding	$t_b = 0.33D$	In accordance with the value of D	
Width of Seadome array	$B = 5D$		
Apron	$A = C_1B$	$C_1 = 0.1$	1
Total width of bedding	$B_L = B+2A$	In accordance with the value of D and A	
Water depth	$h = C_2D$	$C_2 = 0.9, 1.1, 1.3$	3
Incident wave height	$H_i = C_3h$	$C_3 = 0.25, 0.4, 0.55$	3
Wave period	T = (given)	varies	

Tables 1 and 2 provide an overview of the experimental configurations and design parameters used in the study to evaluate the hydrodynamic performance of hemispherical artificial reefs. Table 1 summarizes the governing variables and simulation runs, detailing five configurations (A to E) based on the size of artificial reefs, diameters and numbers of perforations, and total reef widths. It also outlines the water depths and incident wave heights considered across three runs for each configuration, simulating diverse flow and wave conditions. Table 2 presents the designed parameters of seadome characteristics, including the size, total height, basement thickness, and perforation dimensions, along with structural elements like apron width and total bedding width. It also defines water depth, incident wave height, and wave period according to theoretical expressions, ensuring the experimental setup accurately reflects real-world conditions. Together, these tables form the foundation for analyzing the interaction between the reefs and hydrodynamic forces.

4 Result and discussion

4.1 Calibration of the numerical model parameters

To accurately predict the seadome performance factor (SPF) using a numerical model in ANSYS CFD, a cali1bration process was conducted to align the model results with values obtained from field data. The calibration utilized a nomogram, which provides a graphical representation of SPF as a function of key parameters, including relative structure height (D/h) and relative wave length (L/B). This section describes how the numerical model was calibrated by comparing its results to the nomogram data, focusing on matching SPF values for specified configurations.

4.1.1 Data and parameters used in calibration

The nomogram provided SPF values based on field test data for various relative structure heights and relative wave lengths, specifically highlighting the influence of different relative structure heights and relative wave lengths values on SPF(%).

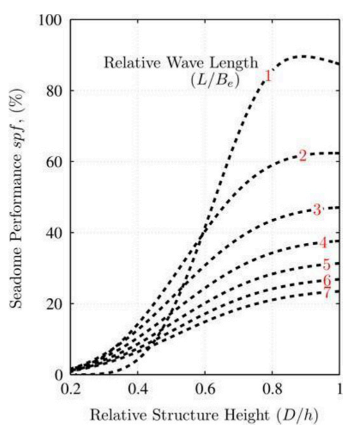

Fig.2. The nomogram serves as a critical tool in the calibration process by providing SPF(%) values derived from field test data

In this study, the calibration process involved validating the numerical model using an independent configuration with a 30 cm wide artificial reef. The results were compared to reference values obtained from a nomogram, as shown in figure 2, to evaluate the model's accuracy and reliability across different reef scales. Following the calibration with the initial data, new simulations were carried out for the 30 cm reef configuration, incorporating varying values of relative structure height (D/h) and wave steepness (Hi/L). The performance of the seadome, represented by the Seadome Performance Factor (SPF), was calculated for cases 1, 2, and 3, yielding values of 85.7487%, 74.3635%, and 63.5242%, respectively, as detailed in table 3, with corresponding Hi/L values.

Table 3. The numerical seadome performance predictions index (%) and the observed values of 30 cm seadome width.

Numerical SPF% with adjusted coefficient	From Nomograph of field studied	RMSD	R^2
85.7487	82.1	2.21	0.924
74.3635	73.2		
63.5242	62.6		

4.2 Validaiton

The validation process involved comparing the results against a separate dataset collected for the 45 cm seadome width under varying conditions (e.g., D/h, L/Be), as shown in Table 4, while using the 30 cm width artificial reef for calibration. The corresponding RMSD and R^2 values demonstrated a strong correlation between the numerical SPF% predictions and the observed values from the nomogram, with minimal average deviation. This indicates that the model predictions for cases 1, 2, and 3 align closely with the field-based nomogram results. Such a close match confirms the numerical model's accuracy for the 30 cm artificial reef configuration and its reliability in predicting the seadome performance factor across different reef widths and environmental conditions. This validation highlights the robustness of the model and its applicability in designing effective coastal protection solutions for varying reef dimensions.

Table 4. The numerical seadome performance predictions index (%) and the observed values from the nomograph of 45 cm seadome width

Numerical SPF% with adjusted coefficient	From Nomograph of field studied	RMSD	R^2
98.4324	94.34	**2.38**	**0.718**
90.8936	90.73		
84.0127	83.56		

4.3 Impact of Configuration and Spacing on Flow Dynamics and Wave Energy Dissipation

To achieve the research objectives, computational fluid dynamics (CFD) simulations were conducted to analyze flow fields represented by velocity profiles for various artificial reef configurations. This study examined the impact of alignment patterns, specifically zigzag and straight configurations, on wake regions downstream of the reef structures. Hemispherical artificial reef units were analyzed with variations in configuration and inter-unit spacing to evaluate their influence on flow behavior and energy dissipation. The distances between the edges of sequential rows of reef units, denoted as Dc1 for the first row, Dc2 for the second, Dc3 for the third, and Dc4 for the fourth row, were systematically varied. Table 5 provides details on the average velocity reduction for different configurations and spacings of straight-aligned seadomes. This approach aimed to assess how inter-row spacing influences wake formation and the overall effectiveness of each configuration in reducing flow velocity and dissipating wave energy.

Table 5. Characteristics of flow for various configurations and spacings of artificial reefs

Configurations	Spacings of seadome				Velocity(m/s)
	Dc1	Dc2	Dc3	Dc4	
Straight alignment	0.075	0.075	0.075	0.075	0.7707
	0.100	0.100	0.100	0.100	0.6526
	0.150	0.150	0.150	0.150	0.5882
Zig-Zag	0.100	0.100	0.100	0.100	0.5332

These calculations involved determining the average flow velocity behind each configuration at a defined distance from the reef units. The configurations tested include zigzag and straight alignments with varying spacing between rows. In each simulation, only the distance between lines (Dc1) to the distance between the edges of the fourth row (Dc4) were varied. From the simulation results, the zigzag configuration with 4 rows perforation of seadomes produced the most effective velocity reduction, achieving a minimum average velocity of 0.5331 m/s at a distance of 4 meters behind the reef units. This corresponds to a 51.54% reduction from the initial velocity of 1.1 m/s, indicating that the staggered arrangement allows for significant wave energy dissipation over a connected, low-velocity wake zone. As the spacing in the straight alignment increased, the effectiveness in reducing flow velocity diminished. With a spacing of 0.1 m between rows, the average velocity increased to 0.6526 m/s, representing a 40.69% reduction. At the widest spacing of 0.15 m, the straight alignment yielded an average velocity of 0.5882 m/s, showing a 46.53% reduction. These results suggest that increasing the row spacing in a straight alignment reduces the overlap between wake zones, leading to higher velocities in the gaps between units and limiting the formation of a unified low-velocity zone.

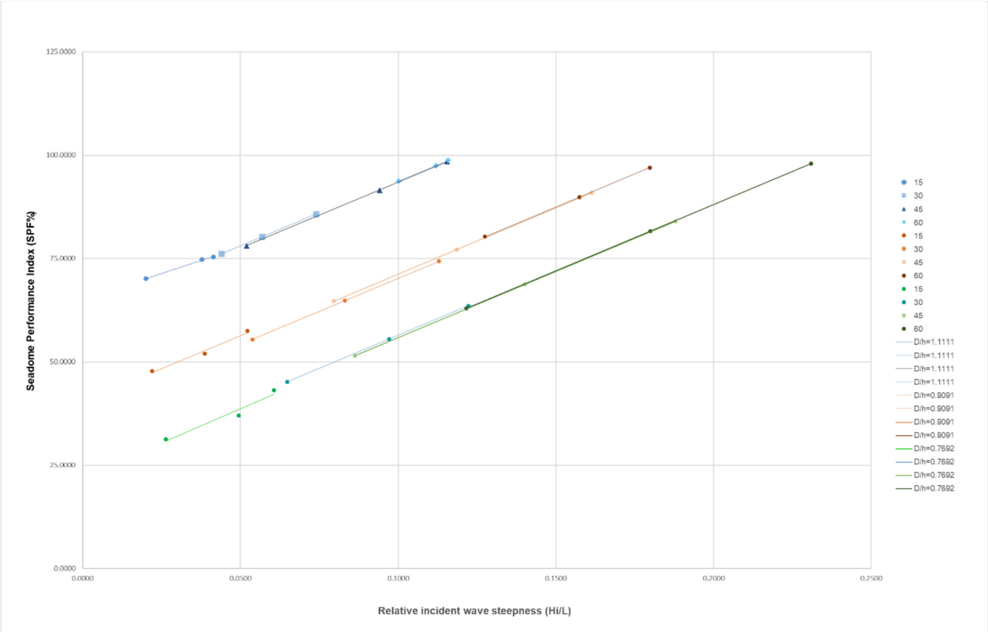

Fig.3. The relationship between seadome performance index (SPF%) and relative incident wave steepness (H_i/L)

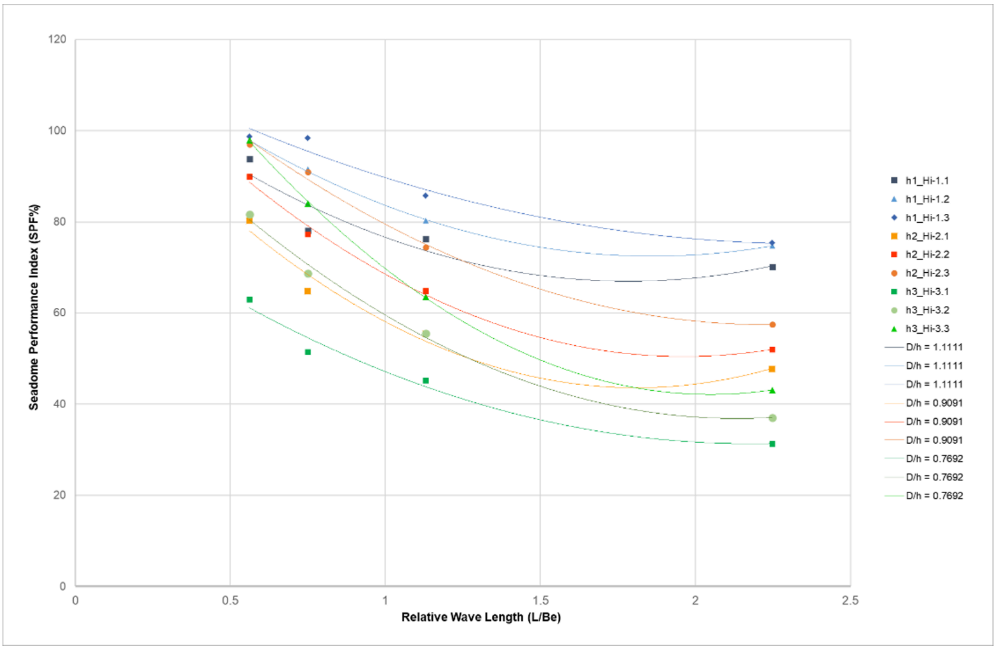

Fig.4. The relationship between seadome performance index (SPF%) and relative wave length(L/B_e)

To investigate the design and optimization of seadome or similar structures and achieve the desired performance levels in varying wave conditions. Can be represented as the relationship between the seadome performance index (SPF%), relative incident wave steepness (H_i/L) and relative wave length(L/B_e) illustrated in figure 3-4 above.

Figure 3 shows that SPF(%) generally decreases as the (L/B_e) ratio increases, showing an inverse relationship. Resulting in relative structure height (D/h) exceeding 1.0, coupled with a relative wavelength (L/B_e) between 0.5 and 1.0, leads to wave amplitude reductions over 90%. And in detail, figure4 the higher D/h ratio achieves a sharp increase in SPF with wave steepness, emphasizing the importance of taller relative structures in enhancing performance.

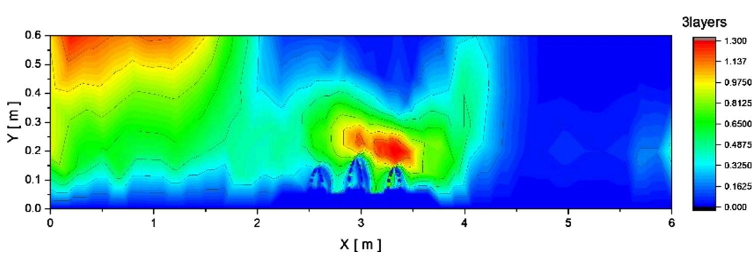

(a) 4 rows perforation at 0.1 spacing of Zig-Zag alignment

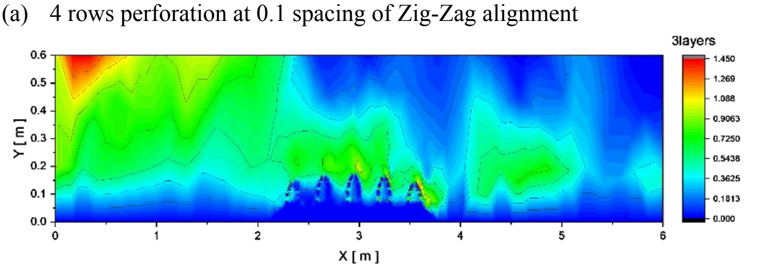

(b) 4 rows perforation at 0.075 spacing of straight alignment

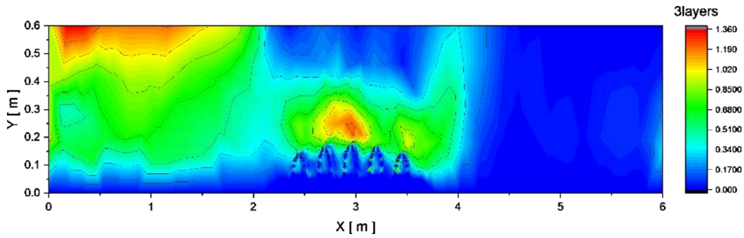

(c) 4 row perforations at 0.10 spacing of straight alignment

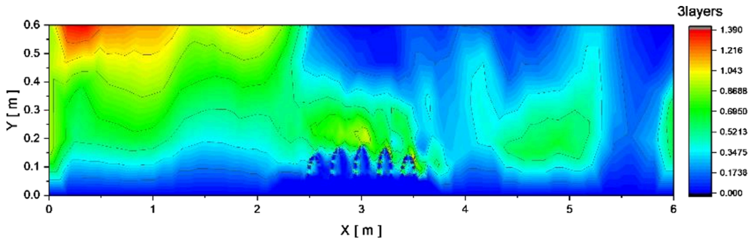

(d) 4 rows perforation at 0.15 spacing of straight alignment

Fig.5. The contour of velocity profile varying the configurations and distances between the edges of the seadome rows of straight alignments R (a) zigzag alignment(b) Dc1=Dc2= Dc3=Dc4=0.075, (c) Dc1=Dc2= Dc3=Dc4=0.10, and (d) Dc1=Dc2= Dc3=Dc4=0.15

Figure 5 represents velocity contour plots for various configurations and spacing distances of seadomes, examining both zigzag and straight alignments to evaluate their effectiveness in reducing flow velocity and controlling wake regions. The tested configurations include a zigzag alignment and straight alignments with spacing distances of 0.075 m, 0.1 m, and 0.15 m between rows (Dc1 = Dc2 = Dc3 = Dc4). The results demonstrate how alignment pattern and spacing influence flow behavior, energy dissipation, and scouring potential.

The zigzag alignment (Figure-5a) creates a continuous, interconnected low-velocity wake region that spans downstream of each seadome unit. This arrangement promotes overlapping wake zones, resulting in a single, expansive low-velocity area that effectively dissipates energy across a larger area. The contour plot reveals extensive green and blue zones in the wake, indicating significant reductions in flow velocity. The staggered layout of the zigzag alignment enhances turbulence, allowing for increased energy dissipation and reducing the likelihood of high-velocity flows that could cause scouring. This configuration is particularly effective for erosion control, as the continuous low-velocity zone encourages sediment stability around the reef structure.

In contrast, the straight alignment configurations exhibit varying levels of effectiveness based on spacing distance. The closest spacing (0.075 m, Figure-5b) achieves a relatively cohesive wake region, with some interaction between adjacent wake zones. The contour plot displays a concentrated area of low velocity immediately downstream of the seadomes, although the wake regions are less interconnected than in the zigzag alignment. This configuration provides effective energy dissipation, but the reduced overlap between wakes results in localized low-velocity zones. The cohesive wake region at this spacing distance helps minimize scouring around the seadome units, as high-velocity flows are limited. As the spacing in the straight alignment increases, the effectiveness of velocity reduction diminishes. The configuration with 0.1 m spacing (Figure-5c) shows distinct, separated wake zones behind each row of seadomes, with moderate flow velocities observed between rows. The contour plot indicates a mixture of low- and moderate-velocity zones, suggesting only partial energy dissipation. This configuration provides a balance between energy dissipation and flow circulation, although it may be less effective for sediment stability compared to the closer spacing.

The widest spacing, 0.15 m (Figure-5d), exhibits the least effective energy dissipation among the configurations. The contour plot shows highly separated wake regions with visible higher velocities between rows. This configuration allows for greater flow velocities to pass between the seadome units, limiting the area of reduced velocity and resulting in isolated wake zones with minimal overlap. Consequently, this spacing distance may increase the potential for localized scouring around the units, as the high-velocity flows can disturb sediment.

In summary, the results highlight the critical role of alignment and spacing in optimizing artificial reef performance. The zigzag alignment is the most effective configuration for reducing flow velocity, creating a large, interconnected low-velocity zone that minimizes scouring risk and supports sediment stability. Among the straight alignment configurations, closer spacings (0.075 m) yield better flow reduction, while wider spacings (0.15 m) result in higher velocities and more isolated wake regions. The wider spacing of 0.15 m may be suitable for applications where flow circulation is desired, but it is less effective in reducing wave energy and protecting against scouring. These findings suggest that the zigzag alignment and closer spacing distances in straight alignments are optimal for enhancing energy dissipation and reducing scouring potential, making them ideal for coastal protection applications.

The wake region is the area downstream of an artificial reef structure. This wake region can include turbulent eddies, low-velocity flow zones and changes in wave patterns, resulting in lower flow velocities and reduced turbulence. Such as sheltered zone provides an ideal habitat for smaller fish species, promoting biodiversity and supporting ecological balance in the surrounding marine environment.

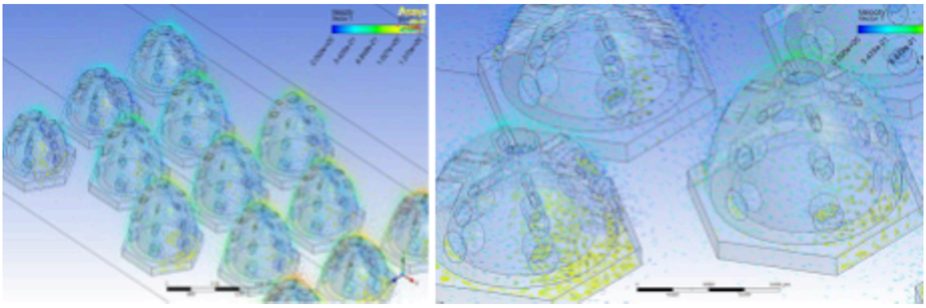

Fig.6. The wake region surrounds by the hemi spherical artificial reefs

This figure 6 shows the vector contours and the detailed the flow direction through seadome. It shows that at base of the structures and within the blue zones behind each dome the contour color is in blue color which mean changes in wave patterns with low velocity and turbulence it called wake region. The recirculating flow in the wake region can help retain plankton and other drifting organisms, making it an attractive feeding ground for filter feeders.

5 Conclusion and Suggestion

5.1 Conclusion

This study highlights the effectiveness of hemispherical artificial reefs, or seadomes, in mitigating wave energy and stabilizing sediments, emphasizing the critical role of alignment and spacing configurations in their performance. The zigzag alignment proved highly efficient, forming interconnected low-velocity wake zones that achieved a 51.54% velocity reduction, lowering the velocity from 1.1 m/s to 0.53 m/s at 4 meters downstream. However, this configuration also increased turbulence intensity, which raised scouring risks and necessitated proper design strategies to mitigate potential drawbacks. In contrast, straight alignments displayed varied performance depending on row spacing. At a spacing of 0.1 m, an average velocity reduction of 40.69% was achieved, with a final velocity of 0.6526 m/s, and moderate wake interaction and erosion risks were observed. Increasing the spacing to
0.15 m improved the velocity reduction to 46.53%, lowering the final velocity to 0.5882 m/s while minimizing turbulence and scouring. Conversely, reducing the spacing to 0.075 m resulted in the highest erosion risks due to intense turbulence and high shear stresses near the structure, although it was effective in dissipating wave energy. Further analysis revealed that a relative structure height (D/h) exceeding 1.0 and a relative wavelength (L/Be) between 0.5 and 1.0 led to wave amplitude reductions of over 90%. Additionally, larger seadomes, with widths ranging from 45 to 60 cm, achieved wave height reductions of up to 98%, highlighting their potential for coastal defense optimization. The study also noted that increasing row spacing in straight alignments diminished wake zone interaction, reducing overall dissipation efficiency. These findings underscore the importance of carefully balancing wake zone dynamics, wave attenuation, sediment transport, and erosion control by tailoring alignment and spacing configurations to meet specific environmental and operational requirements.

5.2 Suggestion for optimal seadome design

To maximize the effectiveness of seadomes in coastal defense, several recommendations emerge from this study. For straight alignments, wider spacing is suggested to reduce scouring while maintaining adequate wave dissipation efficiency. In zigzag alignments, slightly increasing spacing can minimize turbulence overlap while preserving effective energy dissipation. Implementing scour protection measures is essential, especially in high-turbulence configurations, to mitigate erosion risks. Continuous monitoring of seadome performance, sediment dynamics, and flow patterns is crucial to allow for adjustments based on observed changes and environmental conditions. Additionally, optimizing the wake region to dissipate wave energy effectively before it reaches the shoreline is vital for ensuring long-term stability. Balancing sediment transport processes is equally important, as this prevents excessive erosion or deposition, which could undermine the structure's performance. Finally, tailoring the spacing and alignment of seadomes to specific environmental and operational needs will enhance their scalability and effectiveness, making them a robust solution for sustainable coastal management.

References

[1] C. I. Elliff and I. R. Silva, "Coral reefs as the first line of defense: Shoreline protection in face of climate change," 2017, *Elsevier Ltd*. doi: 10.1016/j.marenvres.2017.03.007.

[2] S. M. Cheong, B. Silliman, P. P. Wong, B. Van Wesenbeeck, C. K. Kim, and G. Guannel, "Coastal adaptation with ecological engineering," *Nat Clim Chang*, vol. 3, no. 9, pp. 787–791, Sep. 2013, doi: 10.1038/nclimate1854.

[3] L. Burke, M. D. Spalding, and A. Perry, "Reefs at Risk Revisited," 2011. [Online]. Available: https://www.researchgate.net/publication/263705424

[4] I. I. Na'Im, A. R. M. Shahrizal, and M. D. Safari, "A Short Review of Submerged Breakwaters," in *MATEC Web of Conferences*, EDP Sciences, Sep. 2018. doi: 10.1051/matecconf/201820301005.

[5] H. Dwito Armono, H. D. Armono A, and K. B. Hall, "Wave transmission on submerged breakwaters made of hollow hemispherical shape artificial reefs," 2003. [Online]. Available: https://www.researchgate.net/publication/251314569

[6] K. G. Shirlal, S. Rao, V. Ganesh, and Manu, "Stability of breakwater defenced by a seaward submerged reef," *Ocean Engineering*, vol. 33, no. 5–6, pp. 829–846, Apr. 2006, doi: 10.1016/j.oceaneng.2004.11.017.

[7] C. Srisuwan and P. Rattanamanee, "Modeling of Seadome as artificial reefs for coastal wave attenuation," *Ocean Engineering*, vol. 103, pp. 198–210, May 2015, doi: 10.1016/j.oceaneng.2015.04.069.

[8] W. Seaman, K. Tsukamoto, T. Kawamura, T. Takeuchi, T. D. Beard, and M. J. Kaiser, "Fisheries for Global Welfare and Environment, 5th World Fisheries Congress,"2008.[Online].Available:https://www.researchgate.net/publication/228406611

[9] Y. Belhassen, M. Rousseau, J. Tynyakov, and N. Shashar, "Evaluating the attractiveness and effectiveness of artificial coral reefs as a recreational ecosystem service," *J Environ Manage*, vol. 203, pp. 448–456, Dec. 2017, doi: 10.1016/j.jenvman.2017.08.020.

[10] M. A. A. Rahman *et al.*, "A fundamental cfd investigation of offshore structures for artificial coral reef development," *CFD Letters*, vol. 12, no. 7, pp. 110–125, Jan. 2020, doi: 10.37934/cfdl.12.7.110125.

[11] S. G. Monismith, L. M. M. Herdman, S. Ahmerkamp, and J. L. Hench, "Wave transformation and wave-driven flow across a steep coral reef," *J Phys Oceanogr*, vol. 43, no. 7, pp. 1356–1379, 2013, doi: 10.1175/JPO-D-12-0164.1.

[12] T. S. Hedges, "Regions of validity of analytical wave theories," *Proceedings of the Institution of Civil Engineers: Water, Maritime and Energy*, vol. 112, no. 2, pp. 111– 114, 1995, doi: 10.1680/iwtme.1995.27656.

[13] D. S. Hur, K. H. Lee, and D. S. Choi, "Effect of the slope gradient of submerged breakwaters on wave energy dissipation," *Engineering Applications of Computational Fluid Mechanics*, vol. 5, no. 1, pp. 83–98, 2011, doi: 10.1080/19942060.2011.11015354.

[14] M. Buccino, I. Del Vita, and M. Calabrese, "Engineering Modeling of Wave Transmission of Reef Balls," *J Waterw Port Coast Ocean Eng*, vol. 140, no. 4, Jul. 2014, doi: 10.1061/(asce)ww.1943-5460.0000237.

[15] R. L. Sherman, D. S. Gilliam, and R. E. Spieler, "Artificial reef design: Void space, complexity, and attractants," in *ICES Journal of Marine Science*, Academic Press, 2002. doi: 10.1006/jmsc.2001.1163.

[16] D. H. Yun and Y. T. Kim, "Experimental study on settlement and scour characteristics of artificial reef with different reinforcement type and soil type," *Geotextiles and Geomembranes*, vol. 46, no. 4, pp. 448–454, Aug. 2018, doi: 10.1016/j.geotexmem.2018.04.005.

[17] M. A. A. Rahman, J. Leggoe, K. Thiagarajan, M. H. Mohd, and J. K. Paik, "Numerical simulations of vortex-induced vibrations on vertical cylindrical structure

with different aspect ratios," *Ships and Offshore Structures*, vol. 11, no. 4, pp. 405–423, May 2016, doi: 10.1080/17445302.2015.1013783.

[18] B. S. Baldwin, T. J. Barth, and C. Branch, "A One-Equation Turbulence Transport Model for High Reynolds Number Wall-Bounded Flows."

[19] A. Crivellini and V. D'Alessandro, "Spalart-Allmaras model apparent transition and RANS simulations of laminar separation bubbles on airfoils," *Int J Heat Fluid Flow*, vol. 47, pp. 70–83, 2014, doi: 10.1016/j.ijheatfluidflow.2014.03.002.

[20] R. Ramponi and B. Blocken, "CFD simulation of cross-ventilation flow for different isolated building configurations: Validation with wind tunnel measurements and analysis of physical and numerical diffusion effects," *Journal of Wind Engineering and Industrial Aerodynamics*, vol. 104–106, pp. 408–418, 2012, doi: 10.1016/j.jweia.2012.02.005.

[21] S. N. Ashwindran, A. A. Azizuddin, and A. N. Oumer, "A moment coefficient computational study of parametric drag-driven wind turbine at moderate tip speed ratios," *Australian Journal of Mechanical Engineering*, vol. 20, no. 2, pp. 433–447, 2022, doi: 10.1080/14484846.2020.1714364.